Available online at www.sciencedirect.com
ScienceDirect
Trans. Nonferrous Met. Soc. China 32(2022) 2353−2369
Transactions of Nonferrous Metals Society of China
www.tnmsc.cn

Strength weakening effect of high static pre-stressed granite subjected to low-frequency dynamic disturbance under uniaxial compression

Wu-xing WU[1,2], Feng-qiang GONG[1,2], Quan JIANG[3]

1. Engineering Research Center of Safety and Protection of Explosion & Impact of Ministry of Education (ERCSPEIME), Southeast University, Nanjing 211189, China;
2. School of Civil Engineering, Southeast University, Nanjing 211189, China;
3. State Key Laboratory of Geomechanics and Geotechnical Engineering, Institute of Rock and Soil Mechanics, Chinese Academy of Sciences, Wuhan 430071, China

Received 15 May 2021; accepted 1 November 2021

Abstract: This study aimed to elucidate the strength weakening effect of high static pre-stressed rocks subjected to low-frequency disturbances under uniaxial compression. Based on the uniaxial compressive strength (UCS) of granite under static loading, 70%, 80%, and 90% of UCS were selected as the initial high static pre-stress (σ_p), and then the pre-stressed rock specimens were disturbed by sinusoidal stress with amplitudes of 30%, 20%, and 10% of UCS under low-frequency frequencies (f) of 1, 2, 5, and 10 Hz, respectively. The results show that the rockburst failure of pre-stressed granite is caused by low-frequency disturbance, and the failure strength is much lower than UCS. When the σ_p or f is constant, the specimen strength gradually decreases as the f or σ_p increases. The experimental study illustrates the influence mechanism of the strength weakening effect of high static pre-stress rocks under low-frequency dynamic disturbance, that is, high static pre-stress is the premise and leading factor of rock strength weakening, while low-frequency dynamic disturbance induces rock failure and affects the strength weakening degree.

Key words: deep rock; high static pre-stress; low-frequency dynamic disturbance; strength weakening effect; uniaxial compression; rockburst

1 Introduction

Before the deep rock engineering excavation (mining, tunnels, and nuclear power plants), rocks are restricted to a specific high static pre-stress environment, where the high static pre-stress will always run through the whole excavation process, which is determined by the deep geological environment [1−7]. Deep rock engineering excavation will inevitably produce dynamic disturbances due to mechanical vibration, blasting and impact [8−11], which indicates that rock structures with high static pre-stress are subjected to dynamic disturbances with different amplitudes [12−16]. Furthermore, the deep high static pre-stressed rocks are often subjected to low-frequency dynamic disturbances that induce different degrees of damage, which frequently occurs in deep engineering [8,17−19]. As an example, Fig. 1 [8] presents a schematic diagram of a high static pre-stressed hard rock pillar subjected to low-frequency dynamic disturbance in a deep rock engineering. The mechanical characteristics of rock under this "high static pre-stress (σ_p) + low-frequency dynamic disturbance (σ_d)" stress state may not be analyzed by traditional rock mechanics theory [20−24]. Moreover, there are few research reports on the high static pre-stress rock subjected to low-frequency dynamic disturbance. Therefore, understanding the failure

Corresponding author: Feng-qiang GONG, Tel: +86-18175973819, E-mail: fengqiangg@126.com
DOI: 10.1016/S1003-6326(22)65952-1

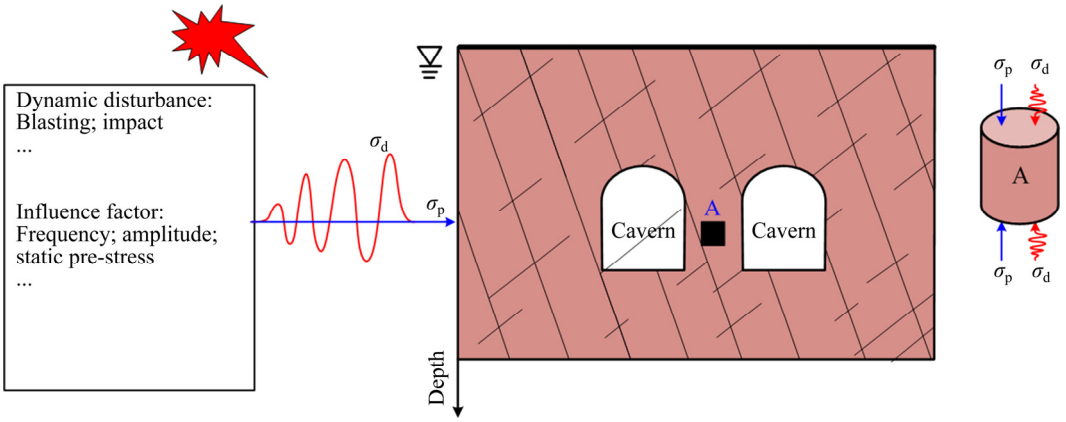

Fig. 1 Schematic diagrams of deep rock stress models (Revised after ZHAO et al [8])

characteristics and mechanisms of high static pre-stressed rock structures subjected to low-frequency dynamic disturbance is deemed to be essential for the design and safe construction in deep rock engineering.

Thus far, many researchers have conducted in-depth studies on the mechanical characteristics of high static pre-stressed rock subjected to impact-dynamic disturbance, such as compression [10,12,13,25−27], tension [28], and fracture [29−31], which have considerably promoted the development of deep rock mechanics theory. For instance, LI et al [10] reported that if the axial pre-compression stress exceeds 70% of uniaxial compressive strength (UCS), the rock strength decreases rapidly under coupled static-impact dynamic loading. GONG et al [25] studied the mechanical properties of red sandstone subjected to impact disturbance at the static pre-stresses of 52%, 70% and 78% of UCS and found that the dynamic strength firstly increases and then decreases as the axial compression ratio increases, and rockburst phenomenon of pre-stressed red sandstone under impact disturbance is also confirmed for the first time. WU et al [28] studied the granite subjected to impact disturbance at the static pre-stresses of 0%, 40%, 80%, 120% and 160% of the static tensile strength and concluded that the dynamic tensile strength increases as the hydrostatic confining pressure increases. These studies have concluded that whether the rock strength decreases or increases is attributed to the static pre-stress and impact dynamic load. However, these efforts mainly concentrated on the rock strength under the coupling of static pre-stress and impact loads with medium or high strain, and the low-frequency dynamic disturbance was seldom considered. As known to all, the deep high pre-stressed rocks are also affected by low-frequency dynamic disturbance, and the superposition of static pre-stress and dynamic disturbances may approach or exceed the static average uniaxial compressive strength of the rock mass, which seriously affects the safety of deep engineering construction. Therefore, in order to reveal the failure of deep rock, it is very important to conduct experimental research on high static pre-stressed rock under the action of low-frequency dynamic disturbance.

To address this deficit in the existing literature and to study the mechanical properties and failure characteristics of high static pre-stress rock materials subjected to low-frequency dynamic disturbances, the high static pre-stressed cylindrical granite specimens subjected to low-frequency dynamic disturbance under the uniaxial compression tests were investigated. In this study, the sum of the σ_p and the dynamic disturbance amplitude range $\Delta\sigma$ was equal to the UCS. Thus, the static pre-stress levels were set to be 70%, 80%, and 90% of UCS, while the corresponding disturbance amplitudes were set to be 30%, 20%, and 10% of UCS, respectively. Moreover, sinusoidal disturbance waves at frequencies of 1, 2, 5, and 10 Hz were selected, respectively. The change characteristics of rock strength were obtained and the failure modes of the high static pre-stressed granite specimens subjected to dynamic disturbance were analyzed. Furthermore, the degree of damage and the distribution characteristics of rock fragments were obtained based on the mass fraction of the double cone and cumulative passing percentage curves; these were used to elucidate the

relationship between rock failure and the high static pre-stress and disturbance frequencies.

2 Experimental

2.1 Preparation of rock specimens

Granite is a commonly encountered rock during deep hard rock engineering projects. In this study, granite, procured from Zhumadian City in Henan Province, China, was used; this granite is hard, homogeneous, and features grey-white stripes. The granite was subjected to an optical micrograph test to determine its composition, and the polarized light micrographs under different magnifications are illustrated in Fig. 2. Table 1 lists the detailed composition and corresponding grain sizes of this granite.

All the granite specimens were processed according to the specifications of the ISRM [32,33]. The cylinder specimens (Fig. 3(a)) with diameter of 50 mm and length of 100 mm were weighed by an electron scale (Fig. 3(b)), the size and flatness were measured by a vernier caliper (Fig. 3(c)), and the wave-velocity was measured by a wave velocimeter (Fig. 3(d)) to select the specimen with the same physical properties for the test to reduce the error. The uniaxial compression tests conducted were following the specifications of ISRM [32,33]. The stress–strain curves of granite are illustrated in Fig. 3(e). As shown, these stress–strain curves are essentially identical, indicating that the granite has good homogeneity. The short post-peak stage of the stress−strain curve indicates that granite specimen has strong rockburst proneness. The failure of granite specimens under uniaxial compression is mainly caused by general shear. The average UCS, elastic modulus, P-wave velocity and density of the three specimens obtained via the tests are listed in Table 2. The average UCS of the specimens was

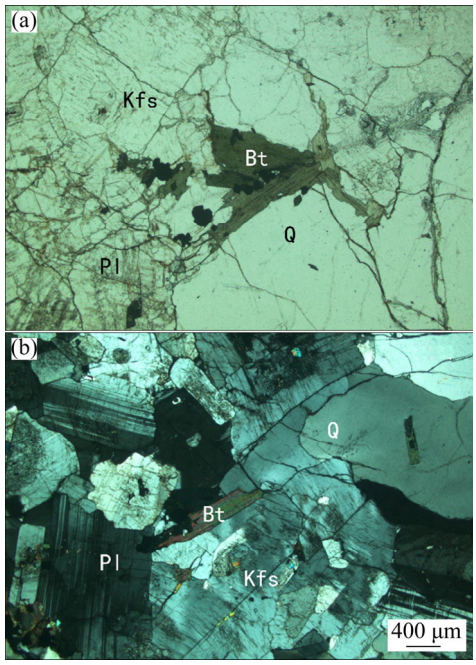

Fig. 2 Polarized light micrographs of granite: (a) Plane-polarized light; (b) Cross-polarized light (Q, Kfs, Pl, and Bt represent quartz, K-feldspar, plagioclase, and biotite, respectively)

Table 1 Composition and grain size of granite

Mineral composition	Content/ wt.%	Grain size/mm
Quartz	33	0.2−1.8
K-feldspar	32	0.2×0.3−1.5×3.0
Plagioclase	30	0.2×0.4−1.8×2.8
Biotite	3	0.03×0.15−0.4×1.2
Sericite	1	0.03×0.06
Opaque mineral	1	0.02−0.2

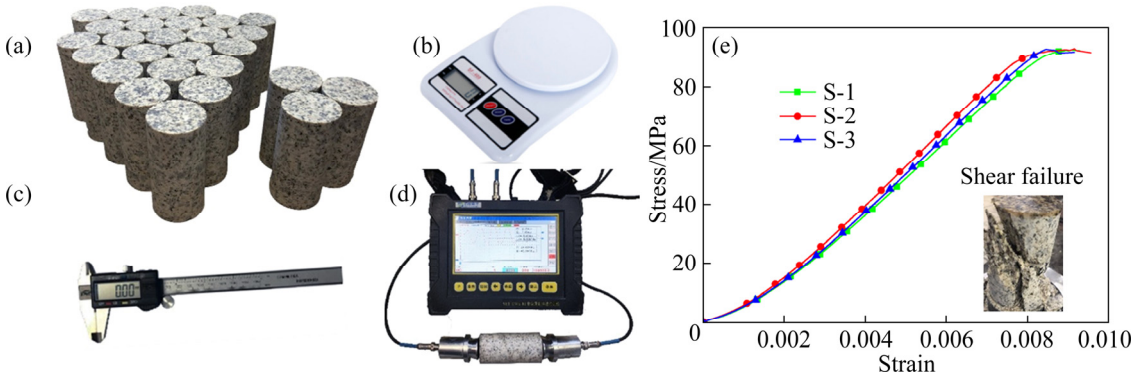

Fig. 3 Granite specimen (a), electronic scale (b), vernier calliper (c), wave velocimeter (d), and stress–strain curves of specimens under uniaxial compression (e)

found to be 92.65 MPa, which corresponds to R4 (strong) in the classification of rock grades suggested by ISRM [34].

Table 2 Basic physical and mechanical characteristics of specimens

Specimen	Density/ (kg·m^{-3})	UCS/ MPa	Elastic modulus/GPa
S-1	2601.69	92.51	5.06
S-2	2602.74	92.71	5.13
S-3	2599.31	92.74	5.17
Average	2601.25	92.65	5.12

2.2 Testing techniques

All uniaxial compression tests under different stress loading conditions were conducted on the MTS−322 test system, as shown in Fig. 4. This test system is mainly composed of the software control system and the equipment loading hardware system, which constitutes a reliable servo-hydraulic closed-loop control equipment system. It includes a rigid loading frame, an axial static and dynamic disturbance system servo device and an automatic data acquisition system (Fig. 4(a)). For better measurements of the axial strain, the MTS axial linear variable differential transformer (LVDT) was installed on the equipment (Fig. 4(b)). When using the MTS−322 system for these tests, firstly, the specimen was loaded to the desired static pre-stress in the axial direction according to the set loading rate, followed by the dynamic disturbance; this sequence is necessary to replicate the conditions of dynamic disturbance acting on the high static pre-stress rock (Fig. 4(c)). The specimens were pre-treated prior to the test by uniformly applying lubricant to both ends to reduce end friction. Additionally, considering the safety factor and the facilitation the collection of rock debris, a protective cover was installed around the specimen to contain the rock fragments created due to specimen failure (Fig. 4(b)).

2.3 Testing plan

Several uniaxial static monotonic loading tests were conducted to determine the average UCS of the specimens, as presented in Fig. 3(e) and Table 2; these results provided a reference for the static pre-stress (σ_p) to be applied and the dynamic disturbance amplitude range ($\Delta\sigma$) in the subsequent

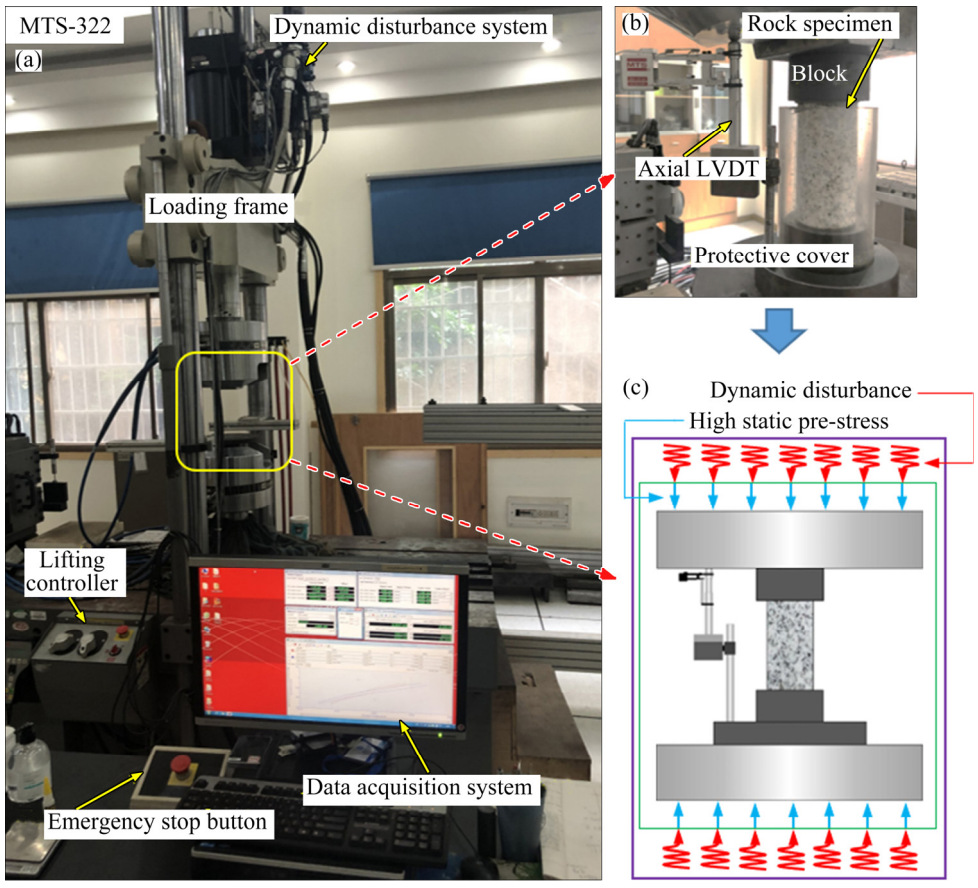

Fig. 4 MTS−322 testing system: (a) Loading system; (b) Rock specimen; (c) Coupling static−dynamic loading

low-frequency dynamic disturbance test of the high static pre-stressed granite under uniaxial compression tests. High static pre-stressed granite subjected to low-frequency dynamic disturbance tests consisted of the static loading stage and dynamic disturbance stage, as shown in Fig. 5. Moreover, the σ_p levels were set as 70%, 80%, and 90% of UCS, and the $\Delta\sigma$ levels were set as 30%, 20%, and 10% of UCS (Fig. 5(a)). Moreover, four different disturbance frequencies (f) of 1, 2, 5, and 10 Hz were adopted for each static pre-stress level (Fig. 5(b)). Table 3 lists the test plan of high static pre-stressed granite specimens subjected to low-frequency dynamic disturbance.

It must be soberly realized that the high-prestressed rock subjected to low-frequency dynamic disturbance test in this work is not the fatigue test. The purpose of this work is to explore the influence of the static pre-stress level, dynamic disturbance, and disturbance frequency on the rock strength when high static pre-stressed rock is subjected to low-frequency dynamic disturbance; rather than the influence of fatigue disturbance and frequency on fatigue life which is concerned in fatigue test. It must be reiterated that our test is essentially different from the fatigue test. We focus on the change characteristics of strength rather than fatigue life.

3 Results and discussion

3.1 Stress–strain curves

Figure 6 presents some typical stress–strain curves of granite under monotonic loading (S-2) and different static pre-stress + dynamic disturbance loading conditions. For each test, the static pre-stress loading stage and the monotonic loading process appear similar, which proves that

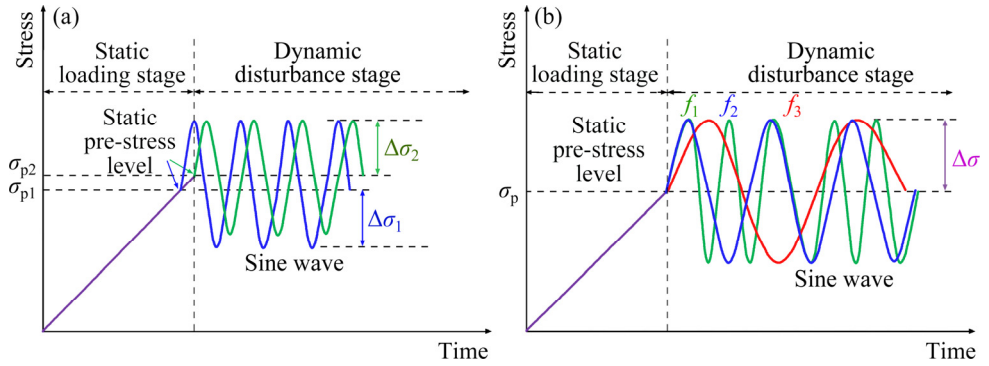

Fig. 5 Testing plan: (a) Same dynamic disturbance frequency for different static pre-stress levels; (b) Different dynamic disturbance frequencies for each static pre-stress level

Table 3 Test plan of high static pre-stressed granite specimens subjected to low-frequency dynamic disturbance

Specimen	Static pre-stress stage		Dynamic disturbance stage		
	Static pre-stress level	σ_p/MPa	Disturbance amplitude	f/Hz	$\Delta\sigma$/MPa
U-70-1	70% UCS	64.86	30% UCS	1	37.06−92.65
U-70-2	70% UCS	64.86	30% UCS	2	37.06−92.65
U-70-5	70% UCS	64.86	30% UCS	5	37.06−92.65
U-70-10	70% UCS	64.86	30% UCS	10	37.06−92.65
U-80-1	80% UCS	74.12	20% UCS	1	55.59−92.65
U-80-2	80% UCS	74.12	20% UCS	2	55.59−92.65
U-80-5	80% UCS	74.12	20% UCS	5	55.59−92.65
U-80-10	80% UCS	74.12	20% UCS	10	55.59−92.65
U-90-1	90% UCS	83.39	10% UCS	1	74.12−92.65
U-90-2	90% UCS	83.39	10% UCS	2	74.12−92.65
U-90-5	90% UCS	83.39	10% UCS	5	74.12−92.65
U-90-10	90% UCS	83.39	10% UCS	10	74.12−92.65

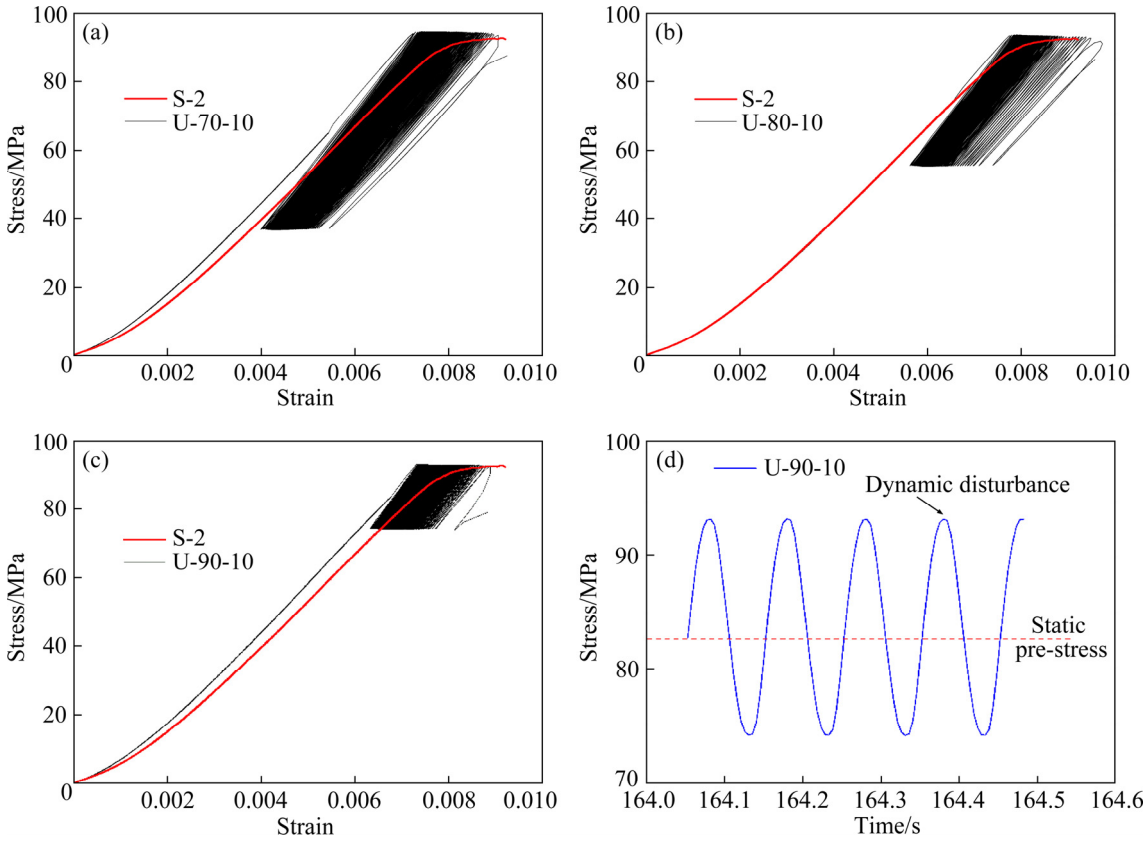

Fig. 6 Stress−strain curves of dynamic disturbance tests with 70% (a), 80% (b) and 90% (c) of UCS, and stress−time curve of U-90-10 (d)

the deformation process essentially remains the same. However, during the dynamic disturbance stage, the slopes of the stress–strain curves become higher than that for the monotonic loading process, which indicates that the deformation is severer during the dynamic disturbance stage. Under the disturbance load, the specimens do not fail immediately after reaching the USC; they fail after several disturbance cycles, and specimen strength is lower than UCS. Furthermore, the number of hysteresis loops in the curve changes from sparse to dense and then back to sparse under dynamic disturbance loading. Compared with monotonic loading up to peak stress level, which is a continuous loading process, the disturbance loading process is a rapid loading−unloading process (Fig. 6(d)). Thus, the specimen is quickly loaded up to the peak stress level and then rapidly unloaded. As a result, the peak stress level only reaches in a very short time; therefore, the specimen does not undergo failure immediately but fails after several disturbance cycles. It can also be seen that rock specimens are basically in the loading stage when they are suddenly destroyed.

3.2 Strength weakening characteristics

Table 4 shows the specimen strength (σ_{ss}) of different high static pre-stressed granite specimens subjected to low-frequency dynamic disturbance as well as the difference between UCS and σ_{ss}. When the σ_p is 64.86 MPa (70% of UCS), the σ_{ss} is respectively 92.27, 89.81, 87.63, and 87.53 MPa for four dynamic disturbance frequencies of 1, 2, 5, and 10 Hz; these values are 0.38−5.12 MPa lower than that under monotonic loading (UCS=92.65 MPa). The specimens under a static pre-stress of 74.12 MPa (80% of UCS) failed at 92.16, 89.73, 87.29, and 86.52 MPa, respectively for the four dynamic disturbance frequencies of 1, 2, 5, and 10 Hz, which are 0.49−6.13 MPa lower than that under monotonic loading. If the σ_p is 83.39 MPa (90% of UCS), the specimens failed at 91.91, 87.79, 84.19, and 79.02 MPa, respectively for the four dynamic disturbance frequencies of 1, 2, 5, and 10 Hz, and these values are 0.74−13.63 MPa lower than that under monotonic loading. On average, the static pre-stressed granites subjected to low-frequency dynamic disturbance conditions indicated that specimen strengths were 6.94, 7.33, and

10.52 MPa lower than the corresponding values under monotonic loading. The abovementioned comparison suggests that the high static pre-stressed granite subjected to low-frequency dynamic disturbance significantly weakens the specimen strength, showing obvious strength weakening effect.

To quantitively describe the strength weakening effect of the high static pre-stressed granite specimens subjected to low-frequency dynamic disturbance, the strength weakening rate (SWR) is proposed. The SWR is defined as follows [17]:

$$\mathrm{SWR}=\frac{\mathrm{UCS}-\sigma_{\mathrm{ss}}}{\mathrm{UCS}}\times 100\%$$

Table 4 Test results under different loading conditions

Specimen	σ_p/MPa	f/Hz	σ_{ss}/MPa	(UCS−σ_{ss})/MPa	SWR/%
U-70-1	64.86 (70% UCS)	1	92.27	0.38	0.41
U-70-2		2	89.81	2.84	3.07
U-70-5		5	87.63	5.02	5.42
U-70-10		10	87.53	5.12	5.53
U-80-1	74.12 (80% UCS)	1	92.16	0.49	0.53
U-80-2		2	89.73	2.92	3.15
U-80-5		5	87.29	5.36	5.79
U-80-10		10	86.52	6.13	6.62
U-90-1	83.39 (90% UCS)	1	91.91	0.74	0.80
U-90-2		2	87.79	4.86	5.25
U-90-5		5	84.19	8.46	9.13
U-90-10		10	79.02	13.63	14.71

The SWR values of different high static pre-stressed granites subjected to low-frequency dynamic disturbance are listed in Table 4. Figure 7 depicts the variation in σ_{ss} with respect to f at different σ_p levels and the relationships between SWR and f. With an increase in f, the decrease trend in σ_{ss} at the σ_p levels of 70% and 80% of UCS is approximately equal; the decrease values under these conditions are 0.41%−5.53% of UCS and 0.53%−6.62% of UCS, respectively. If the specimen is at the σ_p level of 90% of UCS, the decrease value in σ_{ss} is 0.80%−14.71% of UCS, and the strength decrease range is much greater than that of 70% and 80% of UCS. Under different σ_p

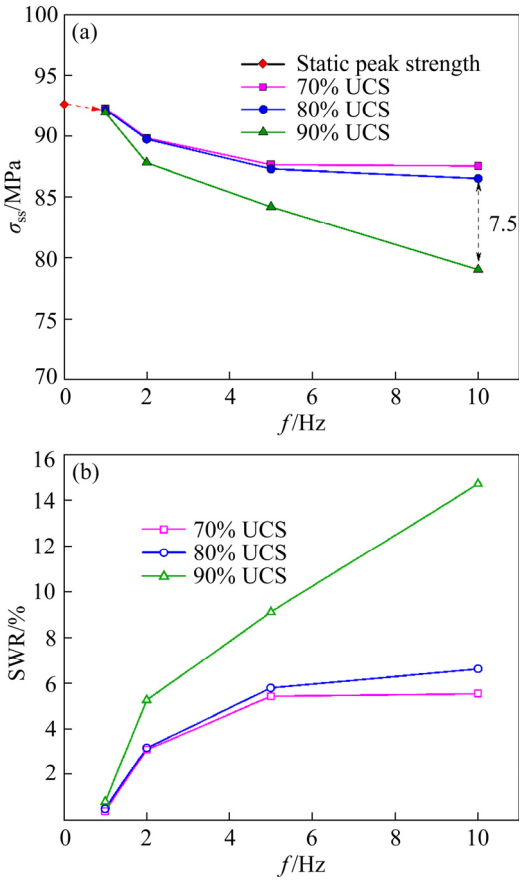

Fig. 7 Variations in σ_{ss} (a) and SWR (b) with change in f under different σ_p levels

levels, the strength weakening rate is different and the σ_p is an inherent factor (i.e., the σ_p of the surrounding rock is always present by itself, not externally applied). Thus, these comparisons indicate that the σ_p is the dominant factor as it determines the strength weakening level. Moreover, the intervals between different σ_p levels vary with respect to f. At f values of 1, 2, 5 and 10 Hz, the specimen strength intervals between σ_p levels of 80% and 90% of UCS are 0.25, 1.94, 3.1, and 7.5 MPa, respectively, whereas those between 70% and 80% of UCS are 0.11, 0.08, 0.34, and 1.01 MPa, respectively (Fig. 7(a)). The strength interval between σ_p levels of 80% and 90% of UCS is greater than that between the σ_p levels of 70% and 80% of UCS; a 7.4-fold difference is observed at 10 Hz. It is interesting to note that the interval between various σ_p is not evident when f=1 Hz; this is also true for the σ_p levels of 70% and 80% of UCS under f=2 Hz and 5 Hz. These phenomena are also reflected in the SWR (Fig. 7(b)). These findings indicate that dynamic disturbances cause significant weakening of the σ_{ss} only when the σ_p

exceeds a certain threshold. Under a constant disturbance frequency, the SWR of granite under three static pre-stress values varies from high to low as follows: 90% of UCS>80% of UCS≈70% of UCS. It is also found that, when the σ_p values are 70% and 80% of UCS, the σ_{ss} exhibits a trend of steep decrease before 5 Hz, followed by a gradual decrease. However, specimen strength decreases sharply as disturbance frequency increases under the σ_p level of 90% of UCS. These results demonstrate that specimen strength decreases more significantly as the disturbance frequency increases at relatively high static pre-stress levels (90% of UCS), as compared to that at lower static pre-stress levels (70% or 80% of UCS).

Figure 8 presents the variation in σ_{ss} with respect to σ_p at different f and the relationships between SWR and σ_p levels. As the σ_p increases from 70% to 90% of UCS, the change in specimen strength under different disturbance frequencies varies. When the disturbance frequency is 1 Hz, the specimen strengths at the σ_p levels of 70%, 80%, and 90% of UCS are 92.27, 92.16, and 91.91 MPa, respectively, which are similar to the average uniaxial compressive strength under monotonic loading (UCS=92.65 MPa), indicating that the increase of σ_p at this frequency has no obvious effect on the strength weakening of specimens. However, with the increase of f, the weakening degree of the σ_{ss} increases significantly with the increase of σ_p. When f increases to 2 Hz, specimen strength is 87.79 MPa at 90% of UCS, which is significantly lower than 89.81 MPa and 89.73 MPa at 70% and 80% of UCS, respectively. These results show that, when f reaches a certain value, the increasing σ_p can promote strength weakening of the specimen. At each f, σ_{ss} for σ_p levels of 70% and 80% of UCS remains almost identical and significantly decreases at 90% of UCS. For instance, when f is 5 Hz, the σ_{ss} is 87.63 and 87.29 MPa at 70% and 80% of UCS (the difference is not significant), respectively; however, at 90% of UCS, it is 84.19 MPa. These findings further demonstrate that σ_p dominates the strength weakening effect and only promotes specimen strength weakening after reaching a certain level. Under a constant σ_p level, the SWR of granite under four disturbance frequencies varies from high to low as follows: f=10 Hz > f=5 Hz > f=2 Hz > f =1 Hz. Particularly, when σ_p is 90% of UCS, the specimen strength is

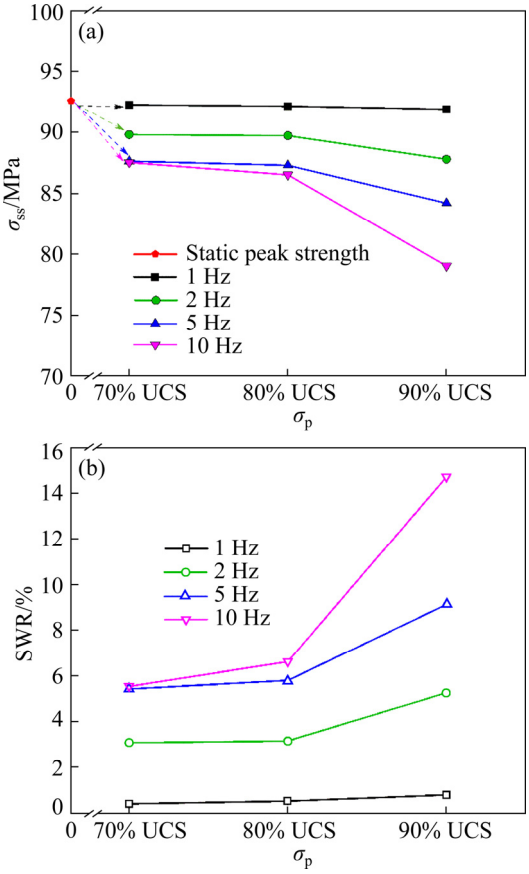

Fig. 8 Variations in σ_{ss} (a) and SWR (b) with change in σ_p under different f levels

91.91, 87.79, 84.19, and 79.02 MPa for disturbance frequencies of 1, 2, 5, and 10 Hz, respectively; the corresponding SWR values are considerably higher than those at other static pre-stress levels. These results imply that, provided σ_p exceeds a certain value, the strength weakening effect increases with the increase of σ_p or f.

In the above comparative analysis, we focus on the analysis of the influence of the static pre-stress level and dynamic disturbance frequency on the strength weakening of rock, which is also the core concern of this paper. Although the disturbance amplitude and dynamic disturbance time under different pre-stress levels may be different, the disturbance amplitude under the same pre-stress is the same, and the variation trend of rock strength under different pre-stress levels is basically the same, which indicates that the conclusion of this paper is reliable.

3.3 Effect of static pre-stress under uniaxial compression

If σ_p reaches a certain threshold, the obvious

strength weakening effect emerges, resulting in a significant decrease in strength. The mechanism of the effect of σ_p can be explained by the stress threshold under the monotonic compression. Figure 9 shows the curves of tangent modulus (E_t) and stress with strain of granite specimen under monotonic loading. E_t gradually increased until the stress reached 40% of UCS and remained basically unchanged. As the strain increased, E_t remained basically unchanged between the stress of 40%−73% of UCS. After that, E_t began to gradually decrease until the stress exceeded 84% of UCS, and E_t began to decrease rapidly until it approached zero. Therefore, combined with the change characteristics of E_t, the failure process of the specimen under monotonic loading can be classified into the following stages and stress thresholds: (I) crack closure stage and crack closure stress (σ_{cc}, and σ_{cc}= 40% UCS), (II) elastic deformation stage and crack initiation stress (σ_{ci}, and σ_{ci}=73% UCS), (III) stable crack growth stage and crack damage stress (σ_{cd}, and σ_{cd}=84% UCS), and (IV) unstable crack expansion stage and failure stress (UCS) (Fig. 9) [35]. As σ_p level in this test is mainly distributed between 70% and 90% of UCS, the effect of these σ_p levels is analyzed.

(1) When σ_p is 64.86 MPa (70% of UCS, E_t= 12.68 GPa), which is in the elastic deformation stage (stress: 40%−73% of UCS), the internal micro-cracks are almost completely closed. Therefore, the stress-wave generated by the dynamic disturbance penetrates the closed crack without reflection, which effectively reduces the weakening of the rock strength caused by the internal crack induced local damage. Similarly, the crack closure reduces the porosity between the mineral particles inside the specimen and enhances the stability of the overall structure of the specimen. Therefore, this shows that only after σ_p reaches a certain level, the dynamic disturbance can induce the significant strength weakening effect.

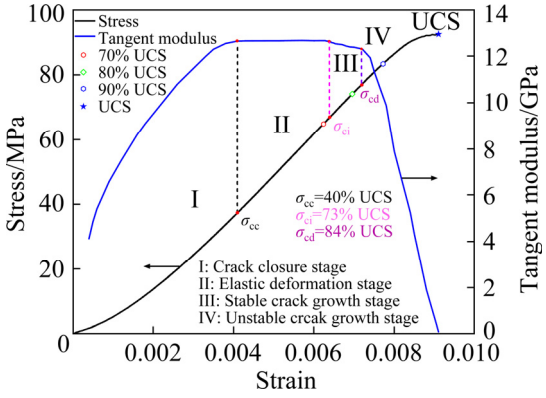

Fig. 9 Stress−strain and tangent modulus−strain curves

(2) When applied σ_p is 74.12 MPa (80% of UCS, E_t=12.41 GPa), the specimen is in the stable crack growth stage (stress: 73%−84% of UCS), and the microcracks that have been closed reopen. A secondary microcrack along the axial direction is generated near the tip of the crack, and the density and length of the microcracks gradually increase with the increase of σ_p level. In the dynamic disturbance stage, the stress-wave propagates along the abundant free-reflection surfaces formed by these cracks and promotes crack propagation and penetration [36]. Therefore, when the static pre-stress falls at this stage, the decrease range of the specimen strength with the increase of the disturbance frequency is slightly larger than that under σ_p in the elastic deformation stage (Figs. 7 and 8). However, due to good homogeneity of granite, the stable crack growth stage is relatively short, resulting in a small change range of tangent modulus, which is basically equal to the elastic stage. Thus, the strength weakening tendency of the specimen is essentially the same as those at static pre-stress levels of 70% and 80% of UCS (Figs. 7 and 8) and the decrease values are 0.41%−5.53% of UCS and 0.53%−6.62% of UCS, respectively (Table 4). It can be considered that the specimen is in a relatively intact state when σ_p is relatively low (such as 70% and 80% of UCS), and the specimen strength does not decrease significantly with the increase of σ_p after dynamic disturbance load. This also indicates that, if σ_p is below certain threshold, the change in f has no notable strength weakening effect.

(3) If σ_p lies in the unstable crack expansion stage, the applied stress exceeds the crack damage threshold (stress: 84% of UCS), and numerous microcracks are generated. Under this static pre-stress state, the density of cracks increases sharply, which dramatically deteriorates the mechanical properties of the rock. Therefore, rock specimens subjected to disturbances at static pre-stress level of 90% of UCS exhibited the lowest strength (Figs. 7 and 8). In particular, when σ_p is 90% of UCS (near the failure state, E_t=10.12 GPa), the lowest specimen strength is 79.02 MPa and the decrease is as high as 14.71% of UCS (f=10 Hz);

in this case, specimen strength decreases significantly with an increase in the disturbance frequency (Fig. 7). These findings demonstrate that, if σ_p exceeds the threshold, dynamic disturbances promote the strength weakening effect and affect the degree of strength reduction.

In summary, the above analysis further emphasizes that σ_p plays a dominant role in the strength weakening process, and on this basis, the disturbance has induced the strength weakening and f affects the degree of strength weakening.

3.4 Failure mode

The failure modes of granite specimens under monotonic and coupled loads are presented in Fig. 10. It is evident that additional cracks and fractured planes are created after the dynamic disturbances, compared with those in the monotonic loading tests. Correspondingly, the specimens mainly undergo general shear failure under monotonic loading (Fig. 10(a)) and conjugate shear failure accompanied by tensile cracks under dynamic disturbance loading (Figs. 10(b−d)). The axial tension cracks on the specimens increase, compared to those under monotonic loading, with the static pre-stress level and dynamic disturbance frequency. As shown in Figs. 10(b) and (c), conjugate shear failure is dominant and accompanied by a small amount of tensile failure. At the static pre-stress level of 90% of UCS, dense tensile and shear cracks are observed; tensile and shear fracture surfaces are also noted on the fragments, which can be attributed to the shear–tensile failure mode (Fig. 10(d)). These phenomena were also observed in previous uniaxial cycle tests [37−39].

In summary, the failure of the specimen is the macroscopic performance after the crack penetrates. Section 3.3 indicates that numerous cracks are generated inside the specimen when σ_p exceeds the crack initiation stress, which affords a large number of free-reflection surfaces for the propagation of disturbing stress-waves (Fig. 9). It can be concluded

Fig. 10 Failure modes of granite specimens: (a) Monotonic loading tests; (b) σ_p level of 70% of UCS; (c) σ_p level of 80% of UCS; (d) σ_p level of 90% of UCS

that the static pre-tress level plays a dominate role in the entire failure process (i.e., determining the internal crack damage), and the dynamic disturbance further promotes crack development and penetration, which can gradually alter the failure mode from general shear failure to conjugate shear failure. During the test, it was also found that the granite specimens would give out violent sound when they were destroyed, which was typical rockburst failure. The occurrence of rockburst in pre-stressed granite under low-frequency disturbance and the occurrence of rockburst in pre-stressed red sandstone under impact disturbance in previous study [25] can be mutually confirmed.

3.5 Failure characteristics

3.5.1 Degree of damage

As the failure mode of the specimen is mainly shear–tension failure, double cones and rock fragments are formed during specimen failure (Fig. 10). To compare the degree of damage of the static pre-stressed specimens subjected to low-frequency dynamic disturbance test and the monotonic loading test, the mass fractions of the double cones and rock fragments are used. The specimens are covered with a protective cover during the test to ensure greater reliability of test data and the conclusions (Fig. 4(b)). Figure 11 describes the average mass fractions of the double cones for specimens under different loading methods. With the increase of σ_p, the mass fraction of the double cones first decreases rapidly and then stabilizes. This reveals that the mass fraction of the rock fragments gradually increases. The average mass fraction of double cones is 45.20% at σ_p level of 90% of UCS, which is 17.64% lower than that of the specimen under the monotonic load. This indicates that the proportion of rock fragments is higher and the damage is severer in the static pre-stressed granite subjected to low-frequency dynamic disturbance. As the granite specimen is brittle, with a UCS of 92.65 MPa (R4), conjugate shear failure occurs after the disturbance test (Fig. 10); this results in additional powder on the fracture surface as compared to that during general shear failure under monotonic loading. Moreover, the conjugate shear failure is also accompanied by tensile failure, which results in several long, strip-shaped fragments, leading to a higher degree of rock fragmentation. This overall trend indicates that the specimen is more prone to damage, which can be severer under dynamic disturbances with high static pre-tress than that during monotonous loading.

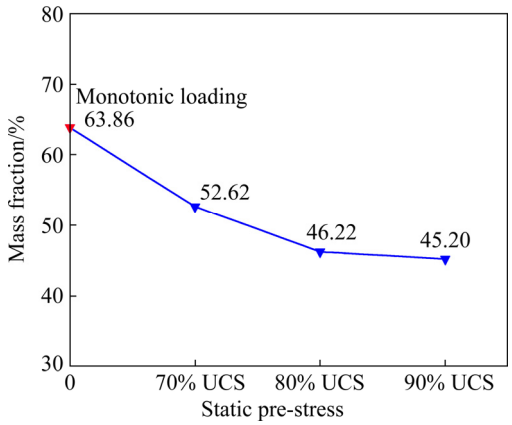

Fig. 11 Overall failure of specimens

3.5.2 Distribution characteristics of rock fragmentation

Rock fragmentation results from the continuous generation, expansion, and penetration of internal cracks. The particle size distribution of a rock can be used to effectively evaluate its crushing efficiency. Therefore, the rock fragments of the high static pre-stressed granite subjected to low-frequency dynamic disturbance tests were screened, and the double cones were excluded. The cumulative mass fraction of rock fragments for a particle size of 0.04−20 mm was determined. Additionally, the uniformity coefficient (C_u) was measured to evaluate the influence of disturbance frequency on rock fragmentation at the same σ_p [39]. The characteristic curves of the particle sizes of the rock fragments are depicted in Fig. 12. It is evident that the cumulative mass fraction curves of the rock fragments of the high static pre-stressed granite subjected to dynamic disturbances exhibited a gradual increase with the increase of disturbance frequency; this indicates that the content of fine particles and the corresponding particle fragmentation mass increase with the increase of disturbance frequency. Moreover, sieving analyses reveal that, as the disturbance frequency increases, the uniformity coefficient increases. For instance, when σ_p reaches 70% of UCS, C_u is 7.55 at 1 Hz, indicating a high grade. However, at 10 Hz (70% of UCS), C_u increases to 29.32, which is 2.8 times more than that at 1 Hz; this indicates that greater amounts of finer fragments are generated at higher

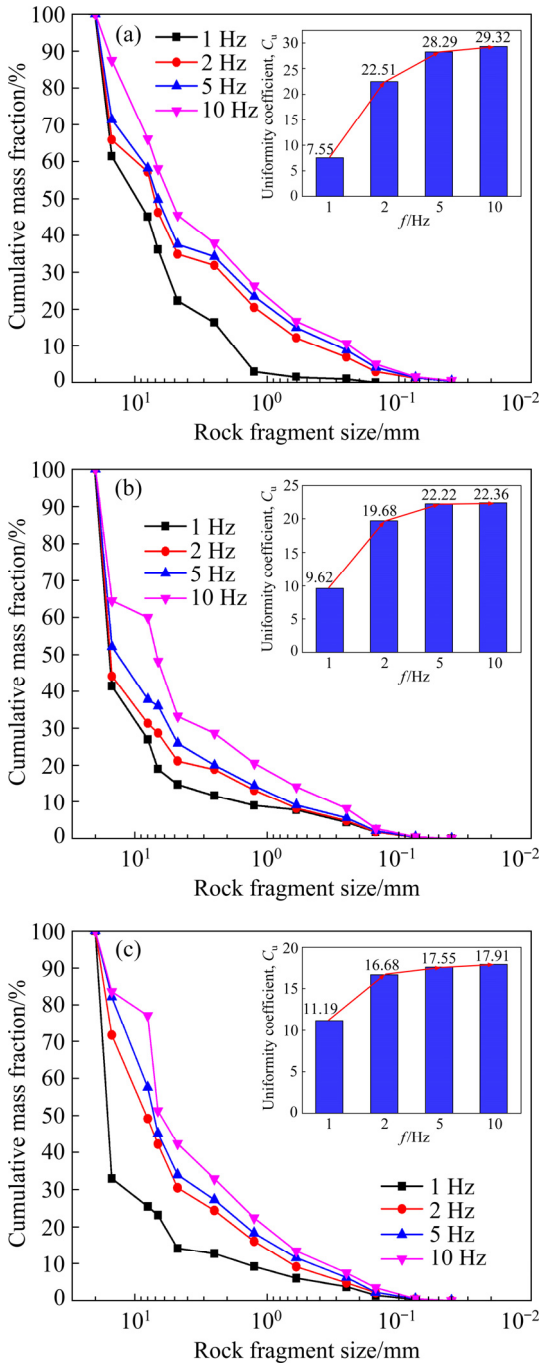

Fig. 12 Particle size distribution of granite fragments: (a) σ_p level of 70% of UCS; (b) σ_p level of 80% of UCS; (c) σ_p level of 90% of UCS

disturbance frequencies. Although the static pre-stress level is different, the cumulative mass fraction curves of the rock fragments and C_u gradually increase with the increase of disturbance frequency. This strongly indicates that the dynamic disturbances are conducive to the rock fragmentation and that there is a greater degree of rock fragmentation at higher frequencies.

Therefore, based on the abovementioned analysis of the degree of specimen damage and the distribution characteristics of rock fragmentation, the failure characteristics of the high static pre-stressed granite under low-frequency dynamic disturbance are obtained. It was found that dynamic disturbances under static pre-stress promote rock damage and the degree of damage is greater than that under monotonic loading. Moreover, the degree of rock fragmentation gradually increases with the increase of disturbance frequency.

4 Discussion

4.1 Strength weakening mechanism

The results demonstrate that notable strength weakening occurs under high static pre-stress and low-frequency dynamic disturbances (Figs. 7 and 8). Moreover, several surrounding rock failures at deep engineering sites indicate the existence of strength weakening effects. For example, when testing the stability of a rock pillar at the Äspö Hard Rock Underground Laboratory (HRL), analyses revealed that the strength of surrounding rock during failure was 54%−63% of UCS, with an average of 59% of UCS [40]. Through the test tunnel of Canadian Underground Laboratory, the rock strength of the mine is approximately 55% of UCS [41]. These findings indicate that the surrounding rock fails before reaching the bearing capacity of its indoor UCS, reflecting a strength weakening phenomenon. Similarly, it has been widely acknowledged that deep surrounding rocks are subjected to high static pre-stress environments and are subsequently damaged when exposed to disturbances. Therefore, research on the strength weakening effect of dynamic disturbance on high static pre-stressed rocks conducted in this paper can provide a certain reference.

The strength weakening of the specimen was mainly influenced by σ_p levels and f, and the SWR also varied. For example, the high static pre-stressed granite under dynamic disturbance tests at 70%, 80%, and 90% of UCS yielded average specimen strengths of 89.31, 88.93, and 85.73 MPa, respectively, which were lower than that under monotonic loading. The decrease in specimen strength can be as high as 14.71% at σ_p level of 90% of UCS (f=10 Hz), more than twice that at σ_p levels of 70% and 80% of UCS (f=10 Hz) (Table 4).

Moreover, the strength weakening of the specimen is significant only when σ_p and f exceed certain values. If σ_p is considerably low, even if f is high, the strength weakening effect may not be apparent. For instance, there was almost no change in the strength interval between the lower σ_p levels of 70% and 80% of UCS (Fig. 7). In general, σ_{ss} decreased as f increased, provided σ_p exceeded a certain level. The strength weakening effect was markedly high for a high static pre-stress and a high disturbance frequency. This is because the higher the loading frequency is, the greater the cumulative damage of rock is, and the more easily the rock fractures [42]. Additionally, the specimen bears a certain axial static pre-stress and undergoes large deformation, resulting in numerous microcracks; this leads to the weakening of the specimen (Fig. 9). Subsequently, σ_{ss} gradually decreases as f increases under the same σ_p (Figs. 7 and 8). These results indicate that σ_p plays a dominant role in strength weakening level, and that disturbance induces strength weakening and f affects the degree of weakening.

Generally, the specimen strength is closely related to its failure mode. The specimen exhibits conjugate shear failure, which is accompanied by tensile failure under coupled high static pre-stress and dynamic disturbances, instead of the general shear failure under monotonic loading (Fig. 10). Under the same static pre-stress level, the specimen undergoes conjugate shear failure at lower disturbance frequencies and shear–tension failure mode as the disturbance frequency increases. Moreover, shear–tension failure is more significant at higher static pre-stress levels and disturbance frequencies. The tensile strength of rock is less than its shear strength. Therefore, the specimen strength under the coupled static pre-stress and dynamic disturbances is lower than that under monotonic loading. Thus, we tentatively suggest that static pre-stress determines whether conjugate shear failure occurs, while dynamic disturbances play the role of inducing this failure (i.e., the transition from shear failure to shear–tension failure). Therefore, the strength weakening effect under static pre-stress and dynamic disturbances can be explained based on the following two aspects: (1) in terms of failure characteristics, the static pre-stress determines the failure mode of the rock, and dynamic disturbances play an inducing role; (2) with regard to the failure mechanism, the static pre-stress dominates the weakening level of rock strength and dynamic disturbances promote this weakening and affect the degree of weakening.

4.2 Comparison of strength weakening effect under tension and fracture failure

In deep engineering, the high static pre-stressed rocks not only suffered from the compression failure, but also tensile and fracture failure [43−46]. Studying the strength characteristics and mechanism of high static pre-stressed rock subjected to dynamic disturbance under tension and fracture failure, is helpful for the construction of deep engineering. For this reason, the dynamic disturbance test was carried out on the static pre-stressed red sandstone to explore the influence of the static pre-stress and dynamic disturbance on the tensile strength and fracture toughness, where the Brazilian disc (BD) specimen was used as the tension test, and in the fracture test the three-point bending specimen with a straight crack in the center (SCB) was used [47,48].

The strength (the tensile strength or fracture toughness) change characteristics and the corresponding strength weakening rate of the static pre-stressed BD and SCB specimens under dynamic disturbance are shown in Figs. 13 and 14, respectively. Whether it is the BD specimen or the SCB specimen under high pre-static load, the specimen strength after being subjected to low-frequency dynamic disturbance is lower than their static strength. As shown in Fig. 13(c), when the pre-static load is 90% of the static tensile failure load (σ_f), the maximum decrease range in SWR is 11.66% (at f = 50 Hz). Meanwhile, the maximum decrease range in SWR is 11.66% (at f = 50 Hz) when pre-static load is 90% of the static fracture failure load (Fig. 14(c)). Moreover, both BD and SCB tests reflect that the greater the pre-static load is, the more significant the strength weakening effect becomes as f increases, which also indicates that the pre-static load level dominates the strength weakening level and the dynamic disturbance further induces the weakening and affects the weakening amplitude. These phenomena also occur in the compression test of this paper. However, the difference is that the pre-static load level has different effects on the strength weakening, that is, one determines the tensile strength weakening level, and the other is the fracture toughness weakening

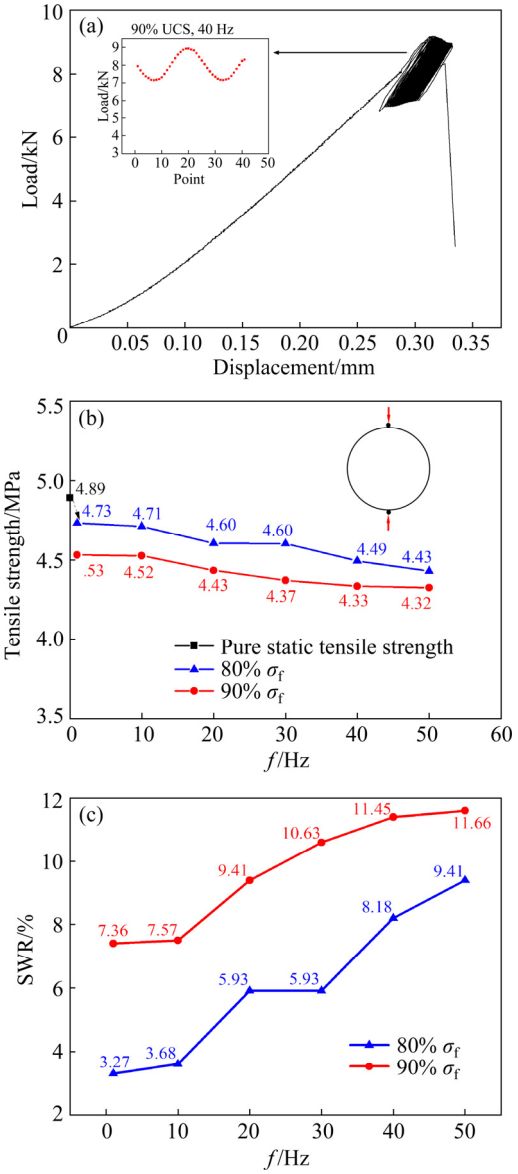

Fig. 13 Test results of BD specimens: (a) Typical actual load−displacement curve [47]; (b) Tensile strength with disturbance frequency; (c) Strength weakening rate with disturbance frequency

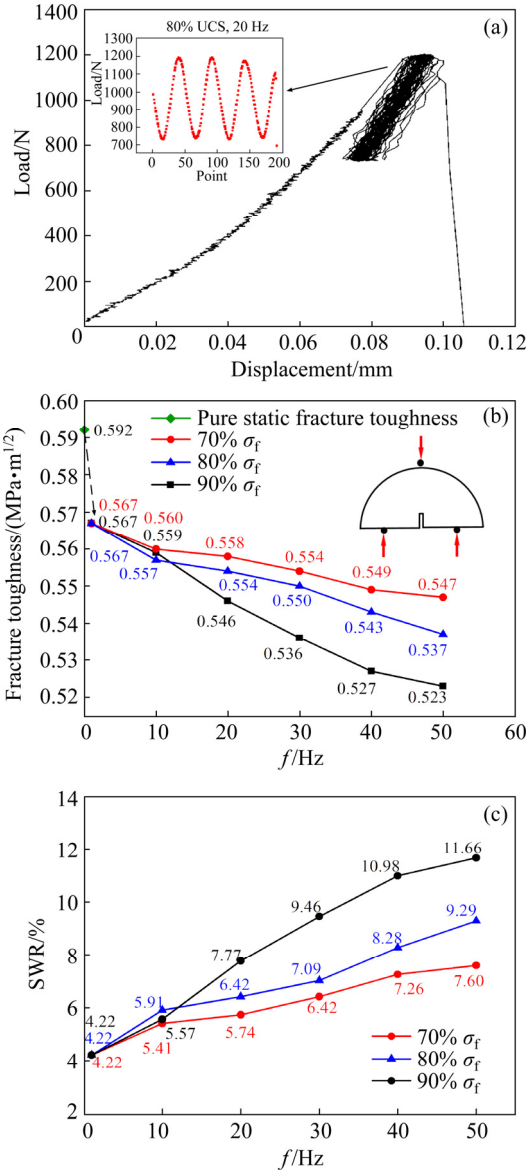

Fig. 14 Test results of SCB specimens: (a) Typical actual load−displacement curve [48]; (b) Fracture toughness with disturbance frequency; (c) Strength weakening rate with disturbance frequency

level. This is mainly due to different stress environments of deep high-stress surrounding rocks, which may cause the failure mode of the rock to be compression, tension or fracture failure.

The above test results further show that when the pre-stress level of the high static pre-stressed rock reaches a certain level and suffers from a certain degree of dynamic disturbance, no matter whether compression, tension or fracture failure occurs, the strength weakening effect will appear. These phenomena can prove that the strength weakening effect of rock may be independent of the stress mode (i.e., compression, tension and fracture), but only related to the stress state of static pre-stress level and the disturbance frequency. Moreover, these test results confirmed that the mechanism of these strength weakening effects is essential that static pre-stress dominates the strength weakening level, while dynamic disturbances can induce the weakening effect and affect the degree of weakening. Furthermore, the strength weakening mechanism can provide a certain theoretical reference for deep underground engineering construction. It is essential to consider and appropriately account for the coupled effect of static pre-stress and low-frequency dynamic

disturbances. In this regard, the magnitude of high static pre-stress (i.e., gravity or tectonic stress) should be monitored and the potential dynamic disturbances due to blasting or impact should be predicted and estimated in advance.

5 Conclusions

(1) The specimen strength of the static pre-stressed granite subjected to the dynamic disturbance is lower than that under static monotonic loading. The higher the static pre-stress level is, the more obvious the strength weakening effect is. The static pre-stress dominates the strength weakening level, and only when the static pre-stress reaches a certain level, the dynamic disturbance can induce the strength weakening and disturbance frequency affects the degree of weakening. Conversely, when the disturbance frequency exceeds a certain value, increasing the static pre-stress level can increase the strength weakening level.

(2) Based on the change of the tangent modulus with loading stress, the failure characteristics of the specimen are analyzed and the stress threshold of each stage is clarified. If the static pre-stress exceeds the crack damage threshold, the internal crack fully expands and penetrates, resulting in a significant weakening of the specimen structure (close to the failure state), which provides a sufficient reflection surface for the disturbing stress-wave, so the specimen strength significantly decreases as the disturbance frequency increases. On the contrary, when the static pre-stress is in the elastic stage or the stable crack growth stage, the internal cracks of the specimen are closed or not fully developed (relatively intact state), which leads to the fact that the specimen strength weakening effect is not obvious.

(3) Based on a comprehensive analysis of the strength, failure mode, and failure characteristics of the specimens, the strength weakening effect of the high static pre-stressed granite subjected to dynamic disturbances can be summarized. The static pre-stress determines the failure mode as shear failure, and the failure mode induced by dynamic disturbance evolves from conjugate shear to shear−tension. The static pre-stress dominates specimen weakening level, while the dynamic disturbances induce strength weakening and affect the degree of weakening.

(4) The high static pre-stressed granite will release kinetic energy when it is destroyed under low-frequency disturbance, which is a typical rockburst phenomenon. The influence of pre-stress level and disturbance frequency on the intensity of rockburst needs further study.

Acknowledgments

This work was financially supported by the National Natural Science Foundation of China (No. 42077244), the Open Research Fund of State Key Laboratory of Geomechanics and Geotechnical Engineering, Institute of Rock and Soil Mechanics, Chinese Academy of Sciences (No. Z020005), and the Fundamental Research Funds for the Central Universities of Southeast University, China (No. 2242021R10080).

References

[1] LI Xi-bing, GONG Feng-qiang, TAO Ming, DONG Long-jun, DU Kun, MA Chun-de, ZHOU Zi-long, YIN Tu-bing. Failure mechanism and coupled static–dynamic loading theory in deep hard rock mining: A review [J]. Journal of Rock Mechanics and Geotechnical Engineering, 2017, 9: 767−782.

[2] BROWN E T, HOEK E. Trends in relationships between measured in-situ stresses and depth [J]. International Journal of Rock Mechanics and Mining Sciences & Geomechanics Abstracts, 1978, 15(4): 211−215.

[3] LI Shao-jun, XIE Zhen-kun, XIAO Ya-xun, FENG Guang-liang, PAN Peng-zhi, WANG Zhao-feng. Review of international research on rock in situ rockmass behavior in deep underground research laboratory [J]. Journal of Central South University(Science and Technology), 2021, 52(8): 2491−2509. (in Chinese)

[4] ZHAO Xing-dong, ZHOU Xin, ZHAO Yi-fan, YU Wen-long. Research status and progress of prevention and control of mining disasters in deep metal mines [J]. Journal of Central South University(Science and Technology), 2021, 52(8): 2522−2538. (in Chinese)

[5] GAO Ming-zhong, XIE Jing, GAO Yan-an, WANG Wen-yong, LI Cong, YANG Ben-gao, LIU Jun-jun, XIE He-ping. Mechanical behavior of coal under different mining rates: A case study from laboratory experiments to field testing [J]. International Journal of Mining Science and Technology, 2021, 31: 825−841.

[6] WANG Qi, JIANG Bei, PAN Rui, LI Shu-cai, HE Man-chao, SUN Hui-bin, QIN Qian, YU Heng-chang, LUAN Yin-cheng. Failure mechanism of surrounding rock with high stress and confined concrete support system [J]. International Journal of Rock Mechanics and Mining Sciences, 2018, 102: 89−100.

[7] LIANG Wei-zhang, ZHAO Guo-yan,WU Hao, CHEN Ying. Optimization of mining method in subsea deep gold mines: A case study [J]. Transactions of Nonferrous Metals Society of China, 2019, 29: 2160−2169.

[8] ZHAO J, ZHOU Y X, HEFNY A M, CAI J G, CHEN S G, LI H B, LIU J F, JAIN M, FOO S T, SEAH C C. Rock dynamics research related to cavern development for ammunition storage [J]. Tunnelling and Underground Space Technology, 1999, 14(4): 513−526.

[9] HUANG R Q, WANG X N. Analysis of dynamic disturbance on rock burst [J]. Bulletin of Engineering Geology and the Environment, 1999, 57(3): 281−284.

[10] LI Xi-bing, ZHOU Zi-long, LOK Tat-seng, HONG Liang, YIN Tu-bing. Innovative testing technique of rock subjected to coupled static and dynamic loads [J]. International Journal of Rock Mechanics and Mining Sciences, 2008, 45(5): 739−748.

[11] DU Kun, LI Xi-bing, LI Di-yuan, WENG Lei. Failure properties of rocks in true triaxial unloading compressive test [J]. Transactions of Nonferrous Metals Society of China, 2015, 25(2): 571−581.

[12] ORTLEPP W D. The behaviour of tunnels at great depth under large static and dynamic pressures [J]. Tunnelling and Underground Space Technology, 2001, 16(1): 41−48.

[13] LU Wen-bo, YANG Jing-hua, YAN Peng, CHEN Ming, ZHOU Chuang-bing, LUO Yi, JIN Li. Dynamic response of rock mass induced by the transient release of in-situ stress [J]. International Journal of Rock Mechanics and Mining Sciences, 2012, 53: 129−141.

[14] LIU K, ZHANG Q B, WU G, LI J C, ZHAO J. Dynamic mechanical and fracture behaviour of sandstone under multiaxial loads using a triaxial Hopkinson bar [J]. Rock Mechanics and Rock Engineering, 2019, 52: 2175−2195.

[15] YIN Zhi-qiang, LI Xi-bing, JIN Jie-fang, HE Xian-qun, DU Kun. Failure characteristics of high stress rock induced by impact disturbance under confining pressure unloading [J]. Transactions of Nonferrous Metals Society of China, 2012, 22: 175−184.

[16] CAI M, KAISER P K. Rockburst phenomenon and support characteristics [M]. Sudbury (Ontario, Canada): Laurentian University Press, 2018.

[17] SI Xue-feng, GONG Feng-qiang. Strength-weakening effect and shear-tension failure mode transformation mechanism of rockburst for fine-grained granite under triaxial unloading compression [J]. International Journal of Rock Mechanics and Mining Sciences, 2020, 131: 104347.

[18] SU Guo-shao, HU Li-hua, FENG Xia-ting, YAN Liu-bin, ZHANG Gang-liang, YAN Si-zhou, ZHAO Bin, YAN Zhao-fu. True triaxial experimental study of rockbursts induced by ramp and cyclic dynamic disturbances [J]. Rock Mechanics and Rock Engineering, 2018, 51(4): 1027−1045.

[19] HU Li-hua, LI Ying-chun, LIANG Xin, TANG Chun-an, YAN Liu-bin. Rock damage and energy balance of strainbursts induced by low frequency seismic disturbance at high static stress [J]. Rock Mechanics and Rock Engineering, 2020, 53(6): 4857−4872.

[20] LI Xi-bing, ZUO Yu-jun, WANG Wei-hua, MA Chun-de, ZHOU Zi-long. Constitutive model of rock under static−dynamic coupling loading and experimental investigation [J]. Transactions of Nonferrous Metals Society of China, 2006, 16: 714−722.

[21] LI X B, LOK T S, ZHAO J, ZHAO P J. Oscillation elimination in the Hopkinson bar apparatus and resultant complete dynamic stress–strain curves for rocks [J]. International Journal of Rock Mechanics and Mining Sciences, 2000, 37(7): 1055−1060.

[22] GONG Feng-qiang, LI Xi-bing, LIU Xi-ling. Preliminary experimental study of characteristics of rock subjected to 3D coupled static and dynamic loads [J]. Chinese Journal of Rock Mechanics and Engineering, 2011, 30(6): 1179−1190. (in Chinese)

[23] ZHANG Q B, ZHAO J. A review of dynamic experimental techniques and mechanical behaviour of rock materials [J]. Rock Mechanics and Rock Engineering, 2014, 47(4): 1411−1478.

[24] LI Xi-bing, GONG Feng-qiang. Research progress and prospect of deep mining rock mechanics based on coupled static-dynamic loading testing [J]. Journal of China Coal Society, 2021, 46(3): 846−866. (in Chinese)

[25] GONG Feng-qiang, LI Xi-bing, LIU Xi-ling, ZHAO J. Experimental study of dynamic characteristics of sandstone under one-dimensional coupled static and dynamic loads [J]. Chinese Journal of Rock Mechanics and Engineering, 2010, 29: 2076−2085. (in Chinese)

[26] LIU K, ZHAO J, WU G, MAKSIMENKO A, HAQUE A, ZHANG Q B. Dynamic strength and failure modes of sandstone under biaxial compression [J]. International Journal of Rock Mechanics and Mining Sciences, 2020, 128: 104260.

[27] LI Shao-jun, XU Huai-sheng, YAN Fei, HUANG Xiang, ZHOU Ji-fang. Experimental study on mechanical properties under dynamics disturbance condition of marble of Jinping deep tunnel [J]. Journal of Central South University (Science and Technology), 2021, 52(8): 2669−2676. (in Chinese)

[28] WU Bang-biao, CHEN Rong, XIA Kai-wen. Dynamic tensile failure of rocks under static pre-tension [J]. International Journal of Rock Mechanics and Mining Sciences, 2015, 80: 12−18.

[29] CHEN Rong, LI Kang, XIA Kai-wen, LIN Yu-liang, YAO Wei, LU Fang-yun. Dynamic fracture properties of rocks subjected to static pre-load using notched semi-circular bend method [J]. Rock Mechanics and Rock Engineering, 2016, 49(10): 3865−3872.

[30] XIE Qin, LI Sheng-xiang, LIU Xi-ling, GONG Feng-qiang, LI Xi-bing. Effect of loading rate on fracture behaviors of shale under mode I loading [J]. Journal of Central South University, 2020, 27(10): 3118−3132.

[31] SHI Dan-dan, CHEN Xu-dong. Flexural tensile fracture behavior of pervious concrete under static preloading [J]. Journal of Materials in Civil Engineering, 2018, 30(11): 06018015.

[32] International Society for Rock Machanics. Suggested methods for determining tensile strength of rock materials [J]. International Journal of Rock Mechanics and Mining Sciences, 1978, 15(3): 99−103.

[33] FAIRHURST C E, HUDSON J A. Draft ISRM suggested method for the complete stress-strain curve for intact rock in uniaxial compression [J]. International Journal of Rock Mechanics and Mining Sciences and Geomechanics Abstracts, 1999, 36(3): 281−289.

[34] BROWN E T. Rock characterization, testing and monitoring: ISRM suggested methods [M]. Oxford: Pergamon, 1981.
[35] MARTIN C D. Seventeenth Canadian geotechnical colloquium: The effect of cohesion loss and stress path on brittle rock strength [J]. Canadian Geotechnical Journal, 1997, 34(5): 698−725.
[36] CADONI E, LABIBES K, ALBERTINI C, BERRA M, GIANGRASSO M. Strain-rate effect on the tensile behaviour of concrete at different relative humidity levels [J]. Materials and Structures, 2001, 34: 21−26.
[37] GERANMAYEH V R, FERDOSI B, OKOTH A D, KUEK B. Strength degradation of sandstone and granodiorite under uniaxial cyclic loading [J]. Journal of Rock Mechanics and Geotechnical Engineering, 2018, 10(1): 117−126.
[38] GERANMAYEH V R, THOENI K, DYSKIN A V, SHARIFZADEH M, SARMADIVALEH M. Strength and damage response of sandstone and granodiorite under different loading conditions of multistage uniaxial cyclic compression [J]. International Journal of Geomechanics, 2020, 20(9): 04020159.
[39] ASTM: D6913/D6913M—17. Standard test methods for particle-size distribution (Gradation) of soils using sieve analysis ASTM [S]. Int West Conshohocken, PA, USA, 2017.
[40] ANDERSSON J C, MARTIN C D, STILLE H. The Äspö pillar stability experiment: Part II—Rock mass response to coupled excavation-induced and thermal-induced stresses [J]. International Journal of Rock Mechanics and Mining Sciences, 2009, 46(5): 879−895.
[41] MARTIN C D, KAISER P K, MCCREATH D R. Hoek−Brown parameters for predicting the depth of brittle failure around tunnels [J]. Canadian Geotechnical Journal, 1999, 36(1): 136−151.
[42] XIA Ming, GONG Feng-qiang. Effects of loading waveforms on rock damage using particle simulation method [J]. Journal of Central South University, 2018, 25(7): 1755−1765.
[43] GONG Feng-qiang, WU Wu-xing, LI Tian-bin, SI Xue-feng. Experimental simulation and investigation of spalling failure of rectangular tunnel under different three-dimensional stress states [J]. International Journal of Rock Mechanics and Mining Sciences, 2019, 122: 104081.
[44] WU Wu-xing, GONG Feng-qiang, YANG Wei-min. Experimental simulation study of spalling in deep rectangular tunnel with plastic fine grain marble [J]. Tunnelling and Underground Space Technology, 2020, 98: 103319.
[45] ZHOU Lei, ZHU Zhe-ming, DONG Yu-qing, YING Peng, WANG Meng. Study of the fracture behavior of mode I and mixed mode I/II cracks in tunnel under impact loads [J]. Tunnelling and Underground Space Technology, 2019, 84: 11−21.
[46] HAN Hao-yu, FUKUDA D, LIU Hong-yuan, SALMI E F, SELLERS E. LIU Ting-jin, CHAN A. Combined finite-discrete element modelling of rock fracture and fragmentation induced by contour blasting during tunnelling with high horizontal in-situ stress [J]. International Journal of Rock Mechanics and Mining Sciences, 2020, 127: 104214.
[47] GONG Feng-qiang, ZHANG Le, LI Xi-bing, LUO Yong. Experimental study on fracture behaviors of hard rock under dynamic disturbance with different pre-static loads [J]. Chinese Journal of Rock Mechanics and Engineering, 2017, 36(8): 1841−1854. (in Chinese)
[48] GONG Feng-qiang, WU Wu-xing, ZHANG Le. Brazilian disc test study on tensile strength-weakening effect of high pre- loaded red sandstone under dynamic disturbance [J]. Journal of Central South University, 2020, 27(10): 2899−2913.

单轴压缩下高静预应力花岗岩受低频动力扰动的强度弱化效应

伍武星[1,2]，宫凤强[1,2]，江 权[3]

1. 东南大学 教育部爆炸与冲击安全防护工程研究中心(ERCSPEIME)，南京 211189；
2. 东南大学 土木工程学院，南京 211189；
3. 中国科学院 岩土力学研究所 岩土力学与岩土工程国家重点实验室，武汉 430071

摘 要：研究高静预应力岩石在单轴压缩下受低频动力扰动的强度弱化机制。根据花岗岩在静态加载下的单轴抗压强度(UCS)，选取 70%、80%和 90%的 UCS 作为初始高静预应力(σ_p)，然后对高静预应力岩石试样施加应力幅值分别为 30%、20%和 10% UCS 的正弦波扰动荷载，其相应低频扰动频率(f)分别为 1、2、5 和 10 Hz。结果表明，高静预应力花岗岩受到低频扰动发生岩爆破坏，其破坏强度远低于静载条件下的单轴抗压强度。当 σ_p 或 f 一定时，花岗岩试样的抗压强度随 f 或 σ_p 的增加而逐渐降低。本研究阐明了低频动力扰动下高静预应力岩石强度弱化效应的影响机理，即高静预应力是岩石强度弱化的前提和主导因素，而低频动力扰动诱发岩石破坏并影响强度弱化程度。

关键词：深部岩石；高静预应力；低频动力扰动；强度弱化效应；单轴压缩；岩爆

(Edited by Wei-ping CHEN)